

Modelling astrophysical fluids with particles

Stephan Rosswog 

Astronomy and Oskar Klein Centre, Stockholm University,
AlbaNova, SE-10691 Stockholm, Sweden
email: stephan.rosswog@astro.su.se

Abstract. Computational fluid dynamics is a crucial tool to theoretically explore the cosmos. In the last decade, we have seen a substantial methodological diversification with a number of cross-fertilizations between originally different methods. Here we focus on recent developments related to the Smoothed Particle Hydrodynamics (SPH) method. We briefly summarize recent technical improvements in the SPH-approach itself, including smoothing kernels, gradient calculations and dissipation steering. These elements have been implemented in the Newtonian high-accuracy SPH code MAGMA2 and we demonstrate its performance in a number of challenging benchmark tests. Taking it one step further, we have used these new ingredients also in the first particle-based, general-relativistic fluid dynamics code that solves the full set of Einstein equations, SPHINCS_BSSN. We present the basic ideas and equations and demonstrate the code performance at examples of relativistic neutron stars that are evolved self-consistently together with the spacetime.

Keywords. hydrodynamics; relativity; stars: neutron; black hole physics; methods: numerical; shock waves

1. Introduction

A large fraction of the matter in the Universe can be modelled as fluids, which makes computational gas dynamics a powerful tool in the theoretical exploration of the Cosmos. While also widespread in engineering applications, *astrophysical* gas dynamics comes with its own set of requirements and these sometimes trigger developments in new directions. Contrary to engineering applications, in astrophysics hard boundary conditions rarely play a role and often additional physical processes beyond pure gas dynamics, e.g. magnetic fields, radiation or nuclear reactions, are main drivers of the evolution. Gravity plays a central role in astrophysical gas dynamics. As a long range force, it can easily accelerate gas to velocities that substantially exceed the local sound speed. Therefore, shocks are ubiquitous in astrophysics, but they only occasionally play a role in engineering applications. As a corollary, an astrophysical gas usually cannot –as in many engineering applications– be treated as “incompressible”, i.e. obeying a $\nabla \cdot \vec{v} = 0$ -condition, and instead the full set of compressible gas dynamics equations needs to be solved. A number of timely astrophysical topics involve gas dynamics in curved spacetime, for example accretion flows around black holes or mergers of neutron stars.

Even if gravity can be accurately treated in the physically rather simple Newtonian approximation, its long-range nature makes it computationally very expensive and the resulting, often filamentary gas structures can pose enormous methodological challenges with respect to geometric adaptivity. To illustrate this in an extreme example, we show in Fig. 1 the tidal disruption of a stellar binary system (67 and 36.8 M_{\odot}) by a supermassive black hole ($10^6 M_{\odot}$), located at the origin (simulation from Rosswog 2020a). Such binary disruptions where actually both components become shredded have been found to make

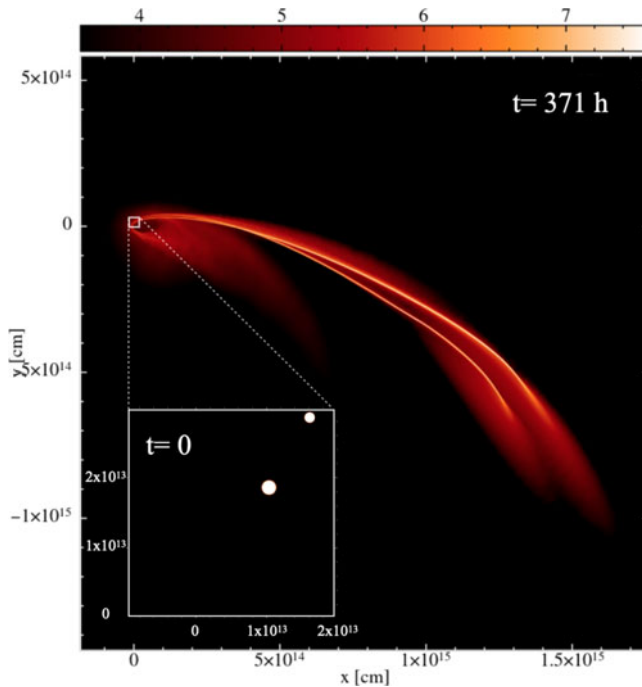


Figure 1. Tidal disruption of a stellar binary system (67 and $36.8 M_{\odot}$) by a $10^6 M_{\odot}$ black hole (located at the origin; color-coded is the column density). About 10% of all stellar tidal disruption events could be disruptions of binary systems (Mandel & Levin 2015). The simulation has been performed with the code MAGMA2 (Rosswog 2020a).

up a non-negligible fraction of all tidal disruption events (Mandel & Levin 2015). The initial configuration of this simulation[†] is shown as inset in the lower left corner. Such a simulation with huge changes in length and density scales, a complicated final geometry with the stars being stretched into extremely thin gas streams that are held together by self-gravity and the majority of the “computational volume” being empty (the initial stars cover $< 10^{-9}$ of the shown volume), are very serious computational challenges. For such applications, particle methods have clear benefits: no additional computational infrastructure (such as an adaptive mesh) is needed, no computational resources are wasted on simulating the vast regions of empty space and the particles simply move where the gas wants to flow. Moreover, the excellent advection properties of particle schemes allow to reliably follow the ejecta out to huge distances.

Methodologically, astrophysical gas dynamics was for a long time split into predominantly Eulerian (mostly Finite Volume) and Lagrangian (mostly Smoothed Particle Hydrodynamics) methods. But in the last decade computational methods have diversified, often combining elements from different methods into “hybrids”. One example of such a hybridization are so-called “moving mesh methods” (Springel 2010; Duffel & MacFadyen 2011; Duffel 2016; Ayache et al. 2022) where space is tessellated into Voronoi-cells. Within these cells familiar Finite Volume techniques such as slope-limited reconstructions are applied and at cell interfaces (either exact or approximate) Riemann solvers are used to determine the numerical inter-cell fluxes. The cells themselves are often moved in a (quasi-)Lagrangian way, but, in principle, they can also be kept fixed in space or move with a velocity that is different from the local fluid velocity. In other words,

[†] The initial conditions for this simulation were kindly provided by I. Mandel and the corresponding stellar profiles by S. Justham.

these are “Adaptive-Lagrangian-Eulerian (ALE)” methods. These methods inherit good shock capturing capabilities and are at the same time highly adaptive and show good (though not perfect) numerical conservation properties.

Such ALE Finite Volume methods, however, are by no means restricted to *non-overlapping* Voronoi cells as basic geometric elements, they can also be applied to freely moving, *overlapping* particles. This has been known in the numerical mathematics community for a long time (see e.g. Ben Moussa, Lanson & Vila 1999; Vila 1999; Hietel, Steiner & Struckmeier 2000; Junk 2003), but has only found its way into astrophysics about a decade ago (e.g. Gaburov & Nitadori 2011; Hopkins 2015; Hubber et al. 2018).

Our main focus here is on the Smoothed Particle Hydrodynamics (SPH) method and its recent developments. We aim at an improved SPH version that keeps the robustness, geometric flexibility and excellent conservation properties of the original method, but is further improved in terms of accuracy. Even more ambitiously, our goal is an accurate particle modelling of a relativistic fluid within a self-consistently evolving, general relativistic spacetime. This goal has recently been reached (Rosswog & Diener 2021) after a string of new elements has been introduced which improve the accuracy of SPH (Rosswog 2010a; Cullen & Dehnen 2010; Rosswog 2010b; Dehnen & Aly 2012; Rosswog 2015b; Frontiere et al. 2017; Rosswog 2020a,b). Most of these new elements are implemented into the Newtonian high-accuracy SPH code MAGMA2 (Rosswog 2020a) which served also as a “test-engine” for many methodological experiments. The new elements have also found their way into the first fully general relativistic, Lagrangian hydrodynamics code SPHINCS_BSSN (Rosswog & Diener 2021).

This paper is organized as follows: in Sec. 2 we discuss the recent improvements that have been implemented into MAGMA2 and we demonstrate its performance in a number of challenging benchmark tests, in Sec. 3 we discuss the method and implementation of the first general relativistic SPH code that consistently solves the full set of Einstein equations and our results are finally summarized in Sec. 4.

2. Recent improvements of Smoothed Particle Hydrodynamics

Here we briefly summarize frequently used SPH equations to set the stage for further improvements and for a smooth transition to the relativistic case which will be described below. A key ingredient of most SPH formulations is the density estimation at the position of a particle a

$$\rho_a = \sum_b m_b W_{ab}(h_a). \quad (2.1)$$

Here m the particle mass, $W_{ab}(h_a) = W(|\vec{r}_a - \vec{r}_b|, h_a)$ is a smooth kernel function, usually with compact support, and h is the “smoothing length” which determines the support size of W . The usual approach is to keep each particle’s mass constant in time so that exact mass conservation is ensured and no continuity equation needs to be solved. One can derive SPH equations elegantly from the SPH-discretized Lagrangian of an ideal fluid (e.g. Monaghan 2005)

$$L = \sum_b m_b \left\{ \frac{1}{2} v_b^2 - u(\rho_b, s_b) - \Phi_b \right\}. \quad (2.2)$$

Here, v_b is the velocity of SPH particle b , u_b its specific internal energy, s_b its specific entropy and Φ_b the gravitational potential. Applying the Euler-Lagrange equations and

the adiabatic form of the first law of thermodynamics,

$$\frac{d}{dt} \frac{\partial L}{\partial \vec{v}_a} - \frac{\partial L}{\partial \vec{r}_a} = 0 \quad \text{and} \quad \left(\frac{\partial u}{\partial \rho} \right)_a = \frac{P_a}{\rho_a^2}, \quad (2.3)$$

yields the SPH momentum equation[†]

$$\frac{d\vec{v}_a}{dt} = - \sum_b m_b \left\{ \frac{P_a}{\rho_a^2} \nabla_a W_{ab}(h_a) + \frac{P_b}{\rho_b^2} \nabla_a W_{ab}(h_b) \right\} + \vec{f}_{g,a} \quad (2.4)$$

with \vec{f}_g being the gravitational acceleration (Price & Monaghan 2007). A consistent energy evolution equation follows in a straight forward way by translating the first law of thermodynamics (see e.g. Rosswog 2009)

$$\frac{du_a}{dt} = \frac{P_a}{\rho_a^2} \sum_b m_b \vec{v}_{ab} \cdot \nabla_a W_{ab}(h_a), \quad (2.5)$$

where $\vec{v}_{ab} = \vec{v}_a - \vec{v}_b$. It is worth mentioning that one has, of course, some freedom in the choice of variables and one can, for example, also evolve the specific thermo-kinetic energy $\hat{e} = u + v^2/2$ according to

$$\frac{d\hat{e}_a}{dt} = - \sum_b m_b \left\{ \frac{P_a \vec{v}_b}{\rho_a^2} \cdot \nabla_a W_{ab}(h_a) + \frac{P_b \vec{v}_a}{\rho_b^2} \cdot \nabla_a W_{ab}(h_b) \right\}. \quad (2.6)$$

As will be seen later, this equation is very similar to the general relativistic evolution equation for the canonical energy per baryon. For practical applications, the energy and momentum equations need to be enhanced by a mechanism to produce entropy in shocks, see Sec. 2.3.

2.1. Kernel function

The kernel function W is a core ingredient of any SPH formulation. Traditionally cubic spline kernels have been used (Monaghan 1992), but they are of moderate accuracy in density and gradient estimates (see e.g. Fig. 4 in Rosswog 2015b) and, for large neighbour numbers, they are prone to a “pairing instability”, where particles begin to form pairs so that resolution is effectively lost. A necessary condition for stability against pairing is the non-negativity the kernel’s Fourier transform (Dehnen & Aly 2012). Wendland (1995) suggested a class of positively definite, radial basis functions of minimal degree and these kernels are immune against the pairing instability.

After exhaustive experiments with various kernels (Rosswog 2015b), we settled for our **MAGMA2** code (Rosswog 2020a) on a C^6 -smooth Wendland kernel (Schaback & Wendland 2006) which overall delivered the best results. For experiments on *static*, perfect lattices other high-order kernels actually delivered density and gradient estimates of even higher accuracy, but in *dynamic* test cases the Wendland kernel was by far superior. This is because it maintains even in dynamical simulations a very regular particle distribution which is crucial for accurate kernel estimates. This kernel, however, needs a large number of neighbour particles in the SPH summations for accurate density and gradient estimates (see e.g. Figs. 4 and 5 in Rosswog 2015b) and so this improvement comes at some computational cost. As a measure to keep the noise level very low, we choose in **MAGMA2** the smoothing length at each time step so that *exactly* 300 neighbour particles contribute in the summations. Technically this is achieved via a very fast tree structure (Gafton & Rosswog 2011), see Rosswog (2020a) for more technical details.

[†] Note that we are neglecting here small corrective terms, usually called “grad-h” terms, see Springel 2002, Monaghan 2002.

2.2. Accurate gradients via matrix-inversion

The standard approach in SPH is to represent the $\nabla P/\rho$ -term on the RHS of the Euler equations via expressions involving gradients of the kernel functions, as shown in Eqs. (2.4) and (2.5). This gradient representation is anti-symmetric, $\nabla_a W_{ab} = -\nabla_b W_{ab}$, and therefore allows for a straight forward enforcement of exact numerical conservation[‡]. While individual gradient estimates can be of moderate accuracy only, the overall simulation may still have a high degree of accuracy since it strictly obeys Nature's conservation laws. It is important, though, that any potential improvement of gradient accuracy does not sacrifice one of SPH's most salient features, its excellent conservation properties.

Such an improvement is actually possible and one way to achieve it is by enforcing the exact reproduction of linear functions via a matrix inversion (Garcia-Senz et al. 2012). In the resulting gradient expression one term (that vanishes for an ideal particle distribution) can be dropped and this omission guarantees the desired anti-symmetry of the gradient expression with respect to the exchanging $a \leftrightarrow b$. This gradient prescription delivers gradient estimates that are several orders of magnitude more accurate than the standard SPH approach, see Fig. 1 in Rosswog (2015b). The new set of SPH equations uses the standard density calculation (2.1), but has momentum and energy equations modified according to[†]

$$\frac{d\vec{v}_a}{dt} = - \sum_b m_b \left\{ \frac{P_a}{\rho_a^2} \vec{G}_a + \frac{P_b}{\rho_b^2} \vec{G}_b \right\}, \quad (2.7)$$

$$\left(\frac{du_a}{dt} \right) = \frac{P_a}{\rho_a^2} \sum_b m_b \vec{v}_{ab} \cdot \vec{G}_a, \quad (2.8)$$

where the gradient functions read

$$\left(\vec{G}_a \right)^k = \sum_{d=1}^3 C^{kd}(\vec{r}_a, h_a) (\vec{r}_b - \vec{r}_a)^d W_{ab}(h_a) \ \& \ \left(\vec{G}_b \right)^k = \sum_{d=1}^3 C^{kd}(\vec{r}_b, h_b) (\vec{r}_b - \vec{r}_a)^d W_{ab}(h_b) \quad (2.9)$$

and the ‘‘correction matrix’’

$$\left(C^{ki}(\vec{r}, h) \right) = \left(\sum_b \frac{m_b}{\rho_b} (\vec{r}_b - \vec{r})^k (\vec{r}_b - \vec{r})^i W(|\vec{r} - \vec{r}_b|, h) \right)^{-1} \quad (2.10)$$

accounts for the local particle distribution. This equation set is based on *much* more accurate gradients, but equally good at numerically conserving physically conserved quantities. This follows directly from the anti-symmetry of the gradient functions with respect to the exchange $a \leftrightarrow b$ and is also confirmed practically in a simulation of the violent collision between two main sequence stars (see Sec. 3.7.3 in Rosswog (2020a)) which is usually considered a worst-case scenario for energy conservation (Hernquist 1993). In this test the conservation accuracy of the matrix inversion approach is on par with the standard SPH formulation.

2.3. Slope-limited reconstruction in the dissipative terms

SPH has a reputation of being overly dissipative, but the SPH equations as derived from the above Lagrangian do not involve any dissipation at all. Therefore, the applied

[‡] Since one uses radial kernels, their gradients point in the directions of the line joining two particles, this ensure angular momentum conservation. See e.g. Sec. 2.4 in Rosswog 2009b for a detailed discussion of conservation in SPH.

[†] In the MAGMA2 code paper we also explore an additional SPH formulation that also uses this accurate gradient prescription.

dissipation is the responsibility of the code developer. One way to add the dissipation that is needed in shocks is, as in typical Finite Volume methods, via Riemann solvers. This approach has occasionally been followed in SPH (Inutsuka 2002; Cha & Whitworth 2003; Cha, Inutsuka & Nayakshin 2010; Puri & Ramachandran 2014), but more common is the use of artificial viscosity. While artificial viscosity is one of the oldest concepts in computational fluid dynamics (von Neumann & Richtmyer 1950), its modern forms are actually not that different from approximate Riemann solvers (e.g. Monaghan 1997).

One way to add artificial viscosity (that is actually very close to the original suggestion of von Neumann & Richtmyer (1950) is to simply enhance the physical pressure P by a viscous contribution Q , i.e. one replaces everywhere $P \rightarrow P + Q$, where the viscous pressure is given by (Monaghan & Gingold 1983; Frontiere et al. 2017)

$$Q_a = \rho_a \left(-\alpha c_{s,a} \mu_a + \beta \mu_a^2 \right), \quad (2.11)$$

and

$$\mu_a = \min \left(0, \frac{\tilde{v}_{ab} \cdot \tilde{\eta}_a}{\eta_a^2 + \epsilon^2} \right), \quad (2.12)$$

$\tilde{v}_{ab} = \vec{v}_a - \vec{v}_b$, $\tilde{\eta}_a$ is the separation vector between particles a and b , de-dimensionalized with particle a 's smoothing length, $\tilde{\eta}_a = (\vec{r}_a - \vec{r}_b)/h_a$. The min-function ensures that the artificial pressure is only applied between approaching particles. The quantity μ_a is a measure of the “velocity jump” between the particles a and b . While this prescription works well in strong shocks, it can be more dissipative than actually needed, especially when there is no shock at all.

This unwanted dissipation can be reduced in a similar way as in Finite Volume methods: rather than applying the velocity jump calculated as the difference of the particle velocities $\vec{v}_a - \vec{v}_b$ (in Finite Volume language: applying a zeroth-order reconstruction between the particles), one can perform a slope-limited reconstruction of the particle velocities from both the a - and the b -side to the mid-point between the two particles and use the jump between these reconstructed velocities at the midpoint when calculating the quantity μ . This different calculation of μ is the only change that is required, otherwise the same equation (2.11) can be used. In MAGMA2 we use a quadratic reconstruction together with a van Leer slope limiter (van Leer 1974; Frontiere et al. 2017), for the technical details we refer to our original code paper (Rosswog 2020a). This reconstruction dramatically reduces unwanted dissipation even if the dissipation parameters α and β are kept at constant, large values. We found this effect particularly pronounced when simulating weakly triggered Kelvin-Helmholtz instabilities: without reconstruction the instability growth was effectively suppressed (as seen in more traditional SPH approaches) while *with* reconstruction the instability grows even at low resolution and with large, constant dissipation parameters α and β at a rate very close to the expected one (see Fig. 20 in Rosswog 2020a).

2.4. Steering dissipation by entropy monitoring

One can go even one step further in reducing dissipation: in addition to the above described slope-limited reconstruction, one can also make the dissipation parameters α and β in Eq. (2.11) time-dependent (Morris & Monaghan 1997; Rosswog et al. 2000; Cullen & Dehnen 2010; Rosswog 2015b). Following Cullen & Dehnen (2010), we calculate in MAGMA2 at each time step for each particle a desired value α^{des} for the dissipation parameter α (we use $\beta = 2\alpha$). If the current value at a particle a , α_a , is larger than α_a^{des} , we let it decay exponentially according to

$$\frac{d\alpha_a}{dt} = -\frac{\alpha_a - \alpha_0}{30\tau_a}, \quad (2.13)$$

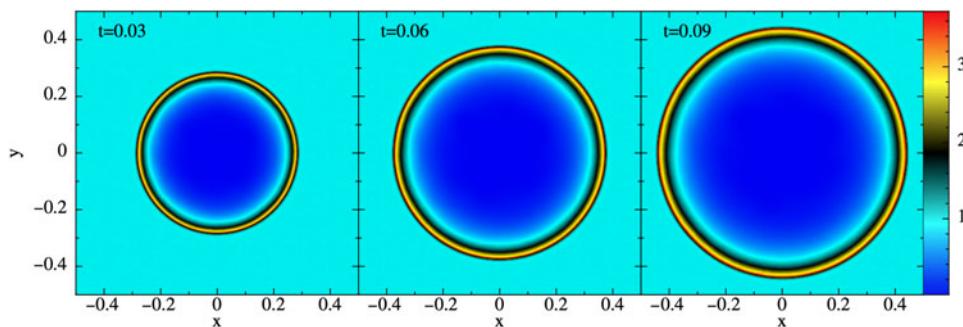


Figure 2. Density evolution in a Sedov-Taylor blast wave. The outermost black ring at the leading edge of the blast is the over-plotted exact solution. Simulation performed with code MAGMA2.

where $\tau_a = h_a/c_{s,a}$ is the particle's dynamical time scale and α_0 is a low floor value (which can be zero). Otherwise, if $\alpha_a^{\text{des}} > \alpha_a$, the value of α_a is instantaneously raised to α_a^{des} .

The novel part in our prescription (Rosswog 2020b) is how we determine α_a^{des} or, in other words, how we determine the exact amount of needed dissipation. The main idea is that we are simulating an ideal fluid which should conserve entropy exactly. In our approach exact entropy conservation is not enforced, so we can monitor it at each particle and use its degree of non-conservation to steer dissipation. A non-conservation of entropy can be the result of a passing shock, or to a much lower extent, it can result from particles becoming noisy for purely numerical reasons. In both cases some amount of dissipation should be applied. For now, we use $s = P/\rho^\Gamma$ as an entropy measure and we monitor over each time step Δt the relative entropy violation $\dot{\xi}_a \equiv (\Delta s_a/\Delta t)/(s_a/\tau_a)$. By numerical experiments we determine a relative entropy violation that can be tolerated without need for dissipation, $\dot{\xi}_0$, and a value $\dot{\xi}_1$, where full dissipation should be applied, in between we smoothly increase the dissipation values, see Rosswog (2020b) for the technical details. This way of steering the dissipation parameter has been found to work very well, it robustly switches on in shocks, but only leads to very low dissipation values otherwise. As an example, we show a Rayleigh-Taylor instability in Fig. 3, where the density (left panel) evolves in very close agreement with literature results (e.g. Frontiere et al. 2017). Non-negligible amounts of dissipation are only triggered in the direct interface between the initial high- and low-density fluid (right panel), elsewhere the dissipation is essentially zero.

2.5. MAGMA2 results

Here we only show a few tests: a Sedov-Taylor explosion as an example for a shock, a Rayleigh-Taylor instability as an instability example and two Schulz-Rinne tests as examples of complex shock-vortex interactions. For a Kelvin-Helmholtz test (density and triggered dissipation) we refer to [a movie on the author's website](#). For more tests and the technical details of a number of benchmark tests we refer to Rosswog (2020a,b).

Sedov blast wave

A classic, multi-dimensional shock problem is the Sedov-Taylor explosion test where a strong, initially point-like blast expands into a low density environment (Sedov 1959; Taylor 1950). For a given explosion energy E , an ambient medium density ρ and polytropic $\Gamma = 5/3$, the blast wave radius propagates according to $r(t) \approx 1.15[(Et^2)/\rho]^{1/5}$ and the density jumps by the strong-explosion limit factor $(\Gamma + 1)/(\Gamma - 1) = 4$. Behind the shock the density drops quickly and finally vanishes at the centre of the explosion. We show in Fig. 2 a cut through the 3D density as a function of time. Also shown

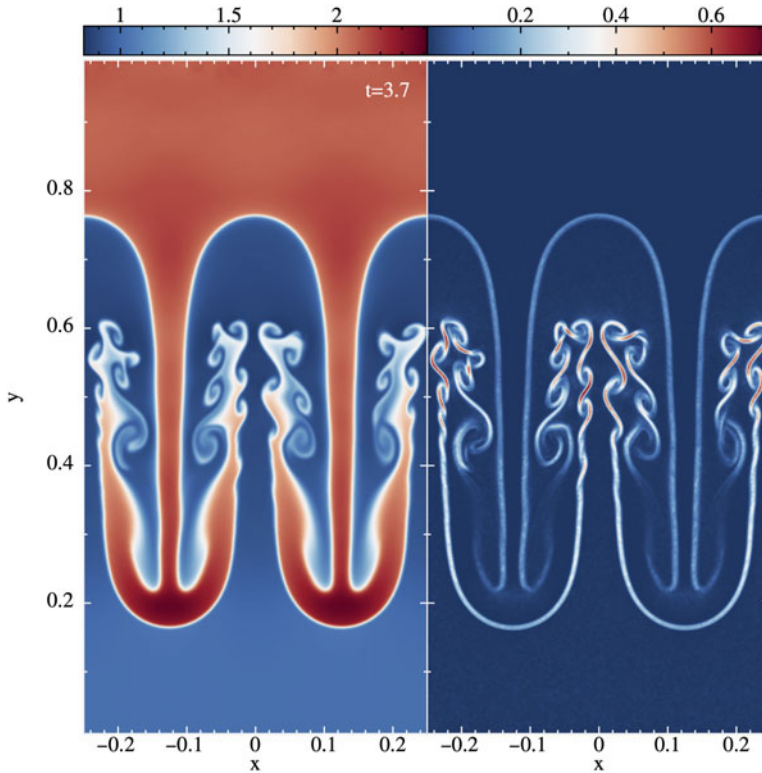


Figure 3. Shown are the density (left) and the applied dissipation parameter α ($\beta = 2\alpha$) as steered via monitoring the local entropy conservation (right) in a Rayleigh-Taylor instability. Note that dissipation is nearly entirely absent throughout most of the flow. Simulation performed with code MAGMA2.

(as leading black circle), but hardly visible, is the exact solution, which demonstrates the accurate agreement between our numerical and the exact solution. No deviation from perfect spherical symmetry is visible and also the particle values are (practically noise-free) lying on top of the exact solution, see Fig. 10 in [Rosswog \(2020a\)](#).

Rayleigh-Taylor test

The Rayleigh-Taylor instability is a standard probe of the subsonic growth of a small perturbation. In its simplest form, a layer of higher density rests on top of a layer with lower density in a constant acceleration field, e.g. due to gravity. While the denser fluid sinks down, it develops a characteristic, “mushroom-like” pattern. Simulations with traditional SPH implementations have shown only retarded growth or even a complete suppression of the instability ([Abel 2011](#); [Saitoh & Makino 2013](#)). We set up this test case as [Frontiere et al. \(2017\)](#) and our MAGMA2 results show a healthy growth of the instability, see Fig. 3, left panel. Note in particular, that our entropy steering triggers dissipation in only a very limited region of space, while the bulk of the simulated volume has essentially no dissipation (right panel).

Schultz-Rinne tests

[Schulz-Rinne \(1993\)](#) designed a particularly challenging set of tests in which initially four constant states meet in one corner and the initial values are chosen so that one elementary wave, either a shock, a rarefaction or a contact discontinuity appears at each

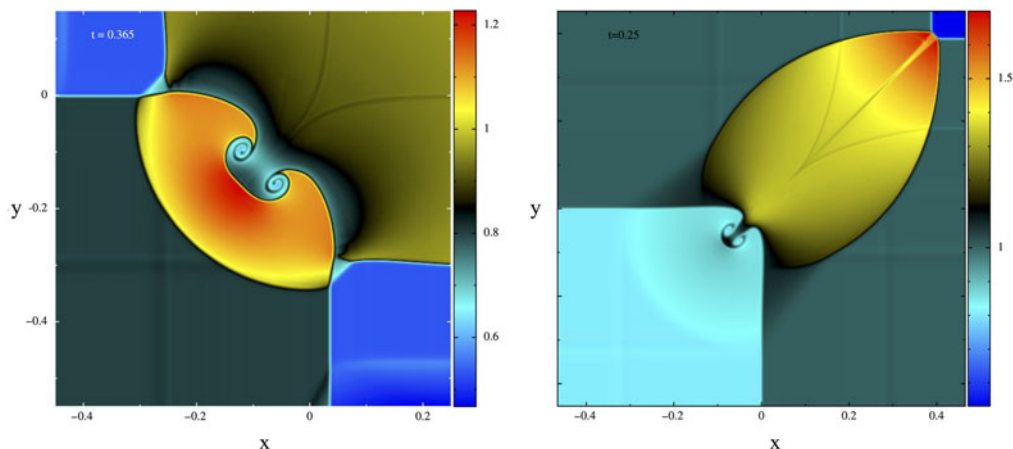


Figure 4. Schulz-Rinne tests. In these challenging tests initially four constant states meet in one corner of the xy -plane. In the subsequent evolution complex shocks and vortex structures form. Our MAGMA2 results are in close agreement with those found in Eulerian simulations.

interface. During the evolution, complex flow patterns emerge, involving shocks and vorticity, for which no exact solutions are known. These tests are considered challenging benchmarks for multi-dimensional hydrodynamics codes (Schulz-Rinne 1993; Lax & Liu 1998; Kurganov & Tadmor 2002; Liska & Wendroff 2003) and we are only aware of one study that tries to tackle these tests with (a Riemann solver version of) SPH (Puri & Ramachandran 2014), with mixed success. We show in Fig. 4 two such tests (produced with the 3D code; 10 particle layers in z - and 660×660 particles in xy -direction; polytropic $\Gamma = 1.4$), for further examples we refer to the MAGMA2 code paper (Rosswog 2020a). Fig. 4 shows crisp and noise-free mushroom-like structures that are in very good agreement with the Eulerian results that can be found in the literature (e.g. Lax & Liu 1998; Liska & Wendroff 2003).

3. Smoothed Particle Hydrodynamics In Curved Spacetime: the SPHINCS_BSSN code

Motivated by the splendid prospects of multi-messenger astrophysics (Rosswog 2015a; Abbott et al. 2017; Barak et al. 2019; Kalogera et al. 2021) our ultimate goal is to develop a general relativistic hydrodynamics code that consistently solves for the evolution of spacetime, but models the fluid with particles. We expect that a particle method has clear benefits (compared to the current Eulerian approaches) in following the small amounts of ejecta, $\sim 1\%$ of the binary mass, that are responsible for the entire electromagnetic display of a compact binary merger.

Since the general relativistic evolution of spacetime is a hyperbolic problem, we need to integrate to spacetime geometry forward in time, while in the Newtonian approach (with an infinite propagation speed of gravity) we solve an elliptic problem where the gravitational forces are calculated from the instantaneous matter state. The methods to evolve spacetime have substantially matured in the last two decades and can be found in recent textbooks on Numerical Relativity (Alcubierre 2008; Baumgarte & Shapiro 2010; Rezzolla & Zanotti 2013; Shibata 2016; Baumgarte & Shapiro 2021), we decided to follow the well-established BSSN-approach for evolving the spacetime on a computational mesh, very similar to what is done in Eulerian approaches, but to evolve matter via Lagrangian particles. This strategy is implemented in our newly developed Numerical Relativity code, SPHINCS_BSSN (Rosswog & Diener 2021).

3.1. General-relativistic hydrodynamics

General relativistic SPH equations can be derived similarly to the Newtonian approach (e.g. Monaghan & Price 2001), see Rosswog (2009), Sec. 4.2 for a step-by-step derivation of the equations that we will use. Instead of discretizing the gas into particles of constant mass, one now assigns to each particle a baryon number ν_b that remains a constant-in-time property of each particle. One chooses a “computing frame” in which the simulations are performed and calculates a computing frame baryon number density at the position of a particle a according to

$$N_a = \sum_b \nu_b W(|\vec{r}_a - \vec{r}_b|, h_a), \tag{3.1}$$

where W is an SPH smoothing kernel (we use the same C^6 -smooth Wendland kernel as in MAGMA2). In other words, we calculate the density N just as the mass density in Newtonian SPH, Eq. (2.1), but with particle masses being replaced with baryon numbers. The number density in the local rest frame density of a particle, n , is related to N via

$$N = \sqrt{-g} \Theta n, \tag{3.2}$$

where g is the determinant of the spacetime metric and the generalized Lorentz factor is given by

$$\Theta \equiv \frac{1}{\sqrt{-g_{\mu\nu} v^\mu v^\nu}} \quad \text{with} \quad v^\alpha = \frac{dx^\alpha}{dt}. \tag{3.3}$$

Similar to the Newtonian approach, one can start from a discretized Lagrangian of an ideal fluid

$$L = - \sum_b \nu_b \left(\frac{1+u}{\Theta} \right)_b. \tag{3.4}$$

Note that we have followed here the convention that we measure all energies in units of the baryon rest mass $m_0 c^2$. We base our numerical evolution variables on the canonical momentum per baryon and the canonical energy per baryon as they follow from the above Lagrangian. The canonical momentum per baryon reads

$$(S_i)_a = (\Theta \mathcal{E} v_i)_a, \tag{3.5}$$

where $\mathcal{E} = 1 + u + P/n$ is the relativistic enthalpy per baryon and the canonical energy per baryon

$$e_a = \left(S_i v^i + \frac{1+u}{\Theta} \right)_a = \left(\Theta \mathcal{E} v_i v^i + \frac{1+u}{\Theta} \right)_a. \tag{3.6}$$

These quantities are evolved in time according to

$$\frac{d(S_i)_a}{dt} = - \sum_b \nu_b \left\{ \frac{P_a \sqrt{-g_a}}{N_a^2} \frac{\partial W_{ab}(h_a)}{\partial x_a^i} + \frac{P_b \sqrt{-g_b}}{N_b^2} \frac{\partial W_{ab}(h_b)}{\partial x_a^i} \right\} + \left(\frac{\sqrt{-g}}{2N} T^{\mu\nu} \frac{\partial g_{\mu\nu}}{\partial x^i} \right)_a \tag{3.7}$$

and

$$\frac{de_a}{dt} = - \sum_b \nu_b \left\{ \frac{P_a \sqrt{-g_a}}{N_a^2} v_b^i \frac{\partial W_{ab}(h_a)}{\partial x_a^i} + \frac{P_b \sqrt{-g_b}}{N_b^2} v_a^i \frac{\partial W_{ab}(h_b)}{\partial x_a^i} \right\} - \left(\frac{\sqrt{-g}}{2N} T^{\mu\nu} \frac{\partial g_{\mu\nu}}{\partial t} \right)_a. \tag{3.8}$$

Note that our equations for the conservation of baryon number, Eq. (3.1), momentum, Eq. (3.7), and Eq. (3.8) (compare to Eq. (2.6)), have a very “Newtonian look and feel”. But while they are very convenient for the numerical evolution, they are actually not the physical variables that we are really interested in, these are n , v^i and u . This means

that we have to recover the physical variables n, v^i, u at every time step from the numerical variables N, S_i and e . But this is a price that also Eulerian approaches have to pay, and we recover the physical variables with very similar methods, see Sec. 2.2.4 in Rosswog & Diener (2021) for the technical details. We also need to add dissipative terms in SPHINCS_BSSN and we follow a strategy similar to the one used in MAGMA2: a) we apply a slope limited reconstruction in the dissipative terms and b) we steer the dissipation by monitoring the entropy change at every particle and time step. The details can be found in Sec. 2.2.3 of Rosswog & Diener (2021).

3.2. Evolving the spacetime via the BSSN formulation

To robustly evolve the spacetime, we have implemented two frequently used variants of the BSSN equations in SPHINCS_BSSN, the “ Φ -method” (Nakamura, Oohara & Kojima (1987); Shibata & Nakamura (1995); Baumgarte & Shapiro (1999)) and the “ W -method” (Tichy & Marronetti (2007); Marronetti et al. (2008)). The complete set of BSSN equations is very lengthy and will therefore not be reproduced here. It is described in detail in a number of Numerical Relativity textbooks (Alcubierre 2008; Baumgarte & Shapiro 2010; Rezzolla & Zanotti 2013; Shibata 2016; Baumgarte & Shapiro 2021) and can also be found in Rosswog & Diener (2021). For all the tests presented here we use the “ Φ -method”.

3.3. Coupling between fluid and spacetime

As can be seen from the hydrodynamic equations Eqs.(3.7) and (3.8), the fluid needs the derivatives of the metric (known on the mesh) at each particle position. The evolution of the metric (evolved on a mesh), in turn, is governed by the energy momentum tensor $T_{\mu\nu}$ that is known at the particle positions. We therefore need to continuously map $T_{\mu\nu}$ from the particles to the mesh (“P2M-step”) and $\partial_\lambda g_{\mu\nu}$ from the mesh to the particles (“M2P-step”).

In the P2M-step we have experimented with methods that are frequently used in particle-mesh methods (Hochney & Eastwood 1988) and with common SPH kernels. But a general relativistic self-gravitating system is numerically very delicate and we did not find these methods accurate enough for our purposes. For example, an initial neutron star setup according to a Tolman-Oppenheimer-Volkoff solution, did not stay close to its equilibrium solution. We found *much* better solutions when using kernels that are frequently used in the context of “vortex methods” (Cottet & Koumoutsakos 2000). These kernels are very accurate for close to uniform particle distributions, but they are not positive definite and they require the cancellation of positive and negative contributions. If applied naively everywhere, this can lead to Gibbs-phenomena-like spurious oscillations near the surface of the star. Therefore we have implemented a hierarchy of kernels of decreasing order with only the least accurate, “parachute” kernel being strictly positive definite. Applying this hierarchy of kernels led to very good results, for details of this approach, we refer to Sec. 2.4 in Rosswog & Diener (2021).

The M2P-step turned out to be less delicate, here we use a quintic Hermite polynomial in generalization of the procedure described in Timmes & Swesty (2000) to ensure that the interpolated values are C^2 when a particle passes from one grid cell to another.

3.4. SPHINCS_BSSN results

Our full evolution code has been scrutinized in a number of standard test cases such as relativistic shock tubes (to test special relativistic hydrodynamics), oscillations of neutron stars in a frozen spacetime (“Cowling approximation”; to test general relativistic hydrodynamics), oscillations of neutron stars when the spacetime is dynamically evolved

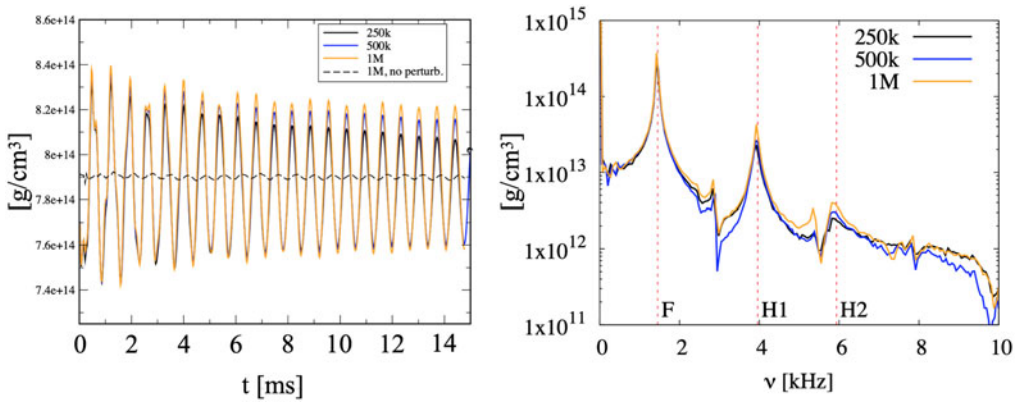


Figure 5. Oscillations of a perturbed neutron star ($\Gamma = 2.0$). Left: central density as function of time. Right: Fourier spectrum of the central density oscillations, the red dashed vertical lines are the fundamental normal mode frequency (F) and the next two higher mode frequencies (H1, H2) as determined by Font et al. (2002). Simulations performed with code SPHINCS_BSSN.

(to test the combined hydrodynamic-plus-spacetime evolution) and last, but not least, the challenging “migration test”. In this test, a neutron star is prepared on the unstable branch and migrates, depending on the type of perturbation, either via violent oscillations onto the stable branch, or collapses into a black hole. In the following, we will only describe the fully relativistic, oscillating neutron star and the migration test. We use units in which $G = c = 1$ and masses are measured in solar units. For the other tests and more details we refer to the original paper (Rosswog & Diener 2021), a first set of neutron star merger simulations with SPHINCS_BSSN can be found in Diener, Rosswog & Torsello (2022).

Oscillating neutron star in a dynamical spacetime

In this test, we set up a $1.40 M_{\odot}$ (gravitational) neutron star, modelled with a polytropic equation of state ($P = Kn^{\Gamma}$; $K = 100$ and $\Gamma = 2.0$; keep in mind our convention of measuring energies in $m_0 c^2$), according to the corresponding Tolman-Oppenheimer-Volkoff (TOV) solution. Subsequently, the star receives a small, radial velocity perturbation and is evolved in its dynamical spacetime. The resulting central density evolution is shown in the left panel of Fig. 5 (for 250 000, 500 000 and 1 million SPH particles). The unperturbed stars stay close to but slightly oscillate (due to truncation error) around the TOV solution (black line). We perturb the stars and measure their oscillation frequencies. The fundamental normal mode (F: 2.696 kHz) and the first two overtones (H1: 4.534 kHz, H2: 6.346 kHz) as determined by Font et al. (2002) via a 3D Eulerian high resolution shock capturing code are shown as the red dashed lines in the right panel. We find excellent agreement of the oscillation frequencies at the $\sim 1\%$ level.

Migration of an unstable neutron star to the stable branch

A more complex test case involves an unstable initial configuration of a neutron star (Font et al. 2002; Cordero-Carrillon et al. 2009; Bernuzzi & Hilditch 2010). According to Eulerian studies, the evolution depends delicately on the star’s initial perturbation: if just evolved, the truncation error alone drives the star to violent oscillations (with $v > 0.5c$) and it finally settles on the stable branch. If, on the other hand, a small radial inward velocity perturbation of only $\delta v_r = -0.005c \sin(\pi r/R)$ is applied, the star collapses and forms a black hole. Can we confirm these results with SPHINCS_BSSN? Yes, we find again very close agreement with the Eulerian studies. Our results for the first case is shown in Fig. 6. The upper panel row shows different stages of the violent oscillation, the lower one

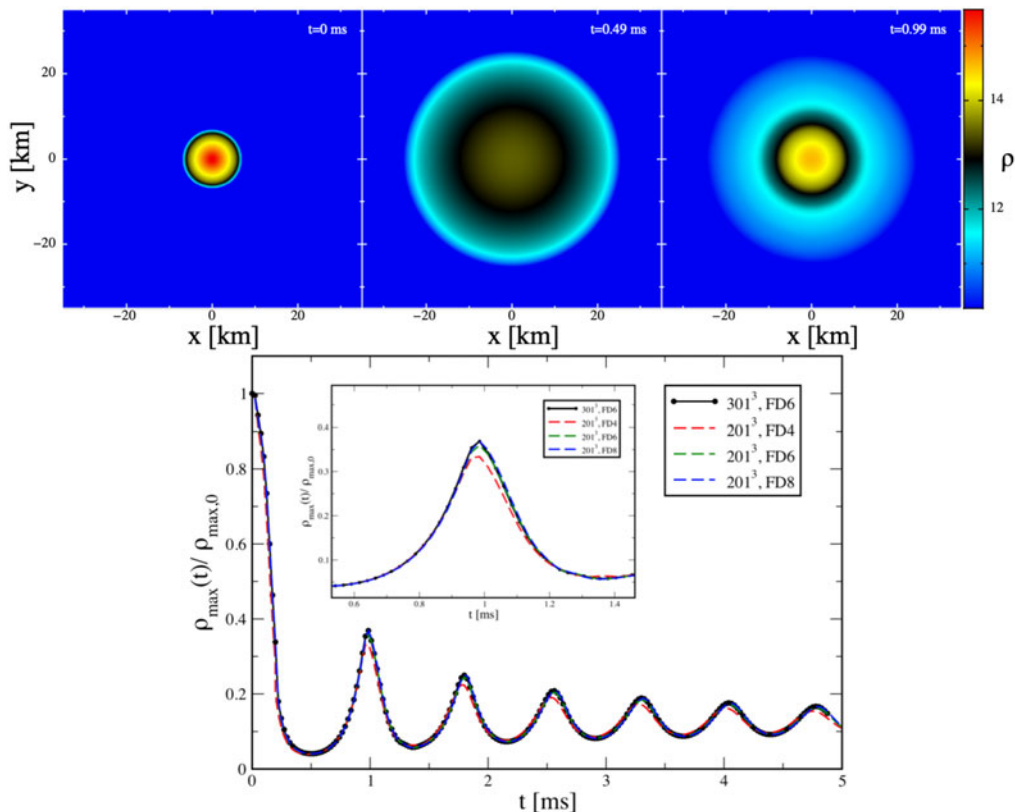


Figure 6. Migration of a neutron star from the unstable to the stable branch. The star evolves, triggered by only truncation error, via violent oscillations ($v > 0.5c$) towards the stable branch. The bottom panel shows the evolution of the central density for different spatial resolutions and Finite Differencing (FD) orders. Simulations performed with code SPHINCS_BSSN.

shows the evolution of the central stellar density (for different numerical resolutions and Finite Difference (FD) orders). When the small inward velocity perturbation is applied, the same star collapses to a black hole, see Fig. 7.

4. Summary and conclusions

In this paper we have described some of the recent developments related to SPH. Our focus was on further improving SPH's accuracy without sacrificing its excellent conservation properties. The new elements include high-order Wendland functions as SPH kernels, accurate gradients that require the inversion of a small matrix and new measures to steer dissipation in SPH. The first of these measures is based on transferring Finite Volume techniques to SPH. More specifically, we perform slope-limited reconstructions between particle pairs and use these reconstructed values in the artificial dissipation terms which massively reduces unnecessary dissipation even if the dissipation parameters are kept at large, constant values. The results can be further improved by additionally making the dissipation parameters time dependent and steer them based on monitoring the exact conservation of entropy.

These new elements have been implemented into two codes that were developed from scratch: the Newtonian code MAGMA2 (Rosswog 2020a) and the fully general relativistic

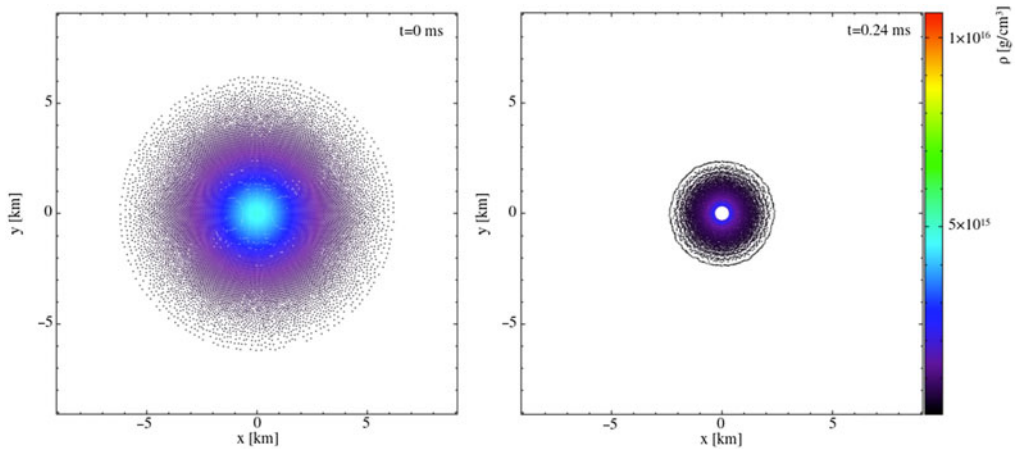


Figure 7. Same star as in the previous figure, but this time a small inward velocity perturbation was applied. This is enough to trigger the collapse to a black hole. Shown are particle positions within $|z| < 0.7$ km. Simulations performed with code SPHINCS_BSSN.

code SPHINCS_BSSN (Rosswog & Diener 2021). Both codes have delivered results of very high accuracy and will be used in our future studies of astrophysical gas dynamics.

Acknowledgements

The author has been supported by the Swedish Research Council (VR) under grant number 2016.03657, by the Swedish National Space Board under grant number Dnr. 107/16, by the research environment grant “Gravitational Radiation and Electromagnetic Astrophysical Transients (GREAT)” funded by the Swedish Research council (VR) under Dnr 2016.06012 and by the Knut and Alice Wallenberg Foundation under grant Dnr. KAW 2019.0112. It is a great pleasure to acknowledge the very productive collaboration with P. Diener, co-developer of SPHINCS_BSSN.

References

- Abbott et al. 2017, *ApJL*, 848, L12
 Abel, T. 2011, *MNRAS*, 413, 271
 Alcubierre, M. 2008, *Introduction to 3+1 Numerical Relativity*, Oxford University Press
 Ayache, E., vanEerten H.J. & Eardly, R., 2022, *MNRAS*, 519, 1315
 Barack et al., 2019, *Classical and Quantum Gravity*, 36, 143001
 Baumgarte, T. & Shapiro, S.L., 1999, *Phys. rev. D*, 59, 024007
 Baumgarte, T. & Shapiro, S.L., 2010, *Numerical Relativity: Solving Einstein’s Equations on the Computer*, Cambridge University Press
 Baumgarte, T. & Shapiro, S.L., 2021, *Numerical Relativity: Starting from Scratch*, Cambridge University Press
 Ben Moussa, B., Lanson, N. & Vila, J.P., 1999, *International Series of Numerical Mathematics*, 29, 31
 Bernuzzi, S. & Hilditch, D., 2010, *Phys. Rev. D*, 81, 084003
 Cha, S.H. & Witworth, A.P., 2003 *MNRAS*, 340, 73
 Cha, S.H., Inutsuka, S.I. & Nayakshin, S., 2010 *MNRAS*, 403, 1165
 Cottet, G.H. & Koumoutsakos, P.D., 2000, *Vortex Methods*, Cambridge University Press, Cambridge
 Cordero-Carrillon, I., et al., 2009, *Phys. Rev. D*, 79, 024017
 Cullen, L. & Dehnen, W., 2010, *MNRAS*, 408, 669
 Dehnen, W. & Aly, H., 2012, *MNRAS*, 425, 1068

- Diener, Rosswog & Torsello, 2022, eprint arXiv:2203.06478
- Duffel, P. & MacFadyen, A., 2011, *ApJS*, 197, 15
- Duffel, P., 2016, *ApJS*, 226, 2
- Font, T. et al., 2002, *Phys. Rev. D*, 65, 084024
- Frontiere, N., Raskin, C & Owen, J.M., 2017, *Journal of Computational Physics*, 332, 160
- Gaburov, E. & Nitadori, K., 2011, *MNRAS*, 414, 129
- Gafton, E. & Rosswog, S., 2011, *MNRAS*, 418, 770
- Garcia-Senz, D., Cabezon, R. & Escartin, J.A., 2012, *A & A*, 538, 9
- Hernquist, L., 1993, *ApJ*, 404, 717
- Hietel, D., Steiner, K. & Struckmeier, J., 2000, *Mathematical Models and Methods in Applied Sciences*, 10, 1363
- Hockney, R.W. & Eastwood, J.W., 1988, *Computer Simulation Using Particles*, McGraw-Hill, New York
- Hopkins, P., 2015, *MNRAS*, 450, 53
- Hubber, P., Rosotti, G.P. & Booth, R.A., 2018, *MNRAS*, 473, 1603
- Inutsuka, S.I., 2002 *Journal of Computational Physics*, 179, 238
- Junk, M., 2003, In: *Griebel M., Schweitzer M.A. (eds) Meshfree Methods for Partial Differential Equations. Lecture Notes in Computational Science and Engineering, vol 26. Springer, Berlin, Heidelberg, 26, 223*
- Kalogera et al., 2022, *The Next Generation Global Gravitational Wave Observatory: The Science Book*, arXiv:2111.06990
- Kurganov, A. & Tadmor, E., 2002 *Numerical Methods for Partial Differential Equations*, 18, 584
- Lax, P. & Liu, X.D., 1998 *SIAM J. Sci. Comput.*, 19, 319
- Liska, R. & Wendroff, B., 2003 *SIAM J. Sci. Comput.*, 25, 995
- Mandel, I., & Levin, Y., 2015, *ApJL*, 805, L4
- Marronetti et al., 2008, *Phys. Rev. D*, 77, 064010
- Monaghan, J.J., 1992, *Ann. Rev. Astron. Astrophys.*, 30, 543
- Monaghan, J.J., 1997, *Journal of Computational Physics*, 136, 298
- Monaghan, J.J. & Price, D.J., 2001, *MNRAS*, 328, 381
- Monaghan, J.J., 2002, *MNRAS*, 335, 843
- Monaghan, J.J., 2005, *Reports on Progress in Physics*, 68, 1703
- Morris, J. & Monaghan, J.J., 1997, *Journal of Computational Physics*, 136, 41
- Nakamura, T., Oohara, K, & Kojima, Y., 1987, *Prog. Theor. Phys. Suppl.*, 90, 1
- Price, D.J. & Monaghan, J.J., 2007, *MNRAS*, 374, 1347
- Monaghan, J.J. & Gingold, R.A., 1983, *Journal of Computational Physics*, 149, 135
- Puri, K. & Ramachandran, P., 2014, *Journal of Computational Physics*, 270, 432
- Rezzolla, L. & Zanotti, O., 2013, *Relativistic Hydrodynamics*, Oxford University Press
- Rosswog, S., et al. 2000, *A&A*, 360, 171
- Rosswog, S., 2009, *New Astronomy Reviews*, 53, 78
- Rosswog, S., 2010a, *Classical and Quantum Gravity*, 27, 114108
- Rosswog, S., 2010b, *Journal of Computational Physics*, 229, 8591
- Rosswog, S., 2015a, *International Journal of Modern Physics D*, 24, 1530012
- Rosswog, S., 2015b, *MNRAS*, 448, 3628
- Rosswog, S., 2015c, *Living Reviews of Computational Astrophysics*, 1, 1
- Rosswog, S., 2020a, *MNRAS*, 498, 4230
- Rosswog, S., 2020b, *ApJ*, 898, 60
- Rosswog, S. & Diener, P., 2021, *Classical and Quantum Gravity*, 38, 115002
- Saitoh, T.R. & Makino, J., 2013, *ApJ*, 768, 44
- Schaback, R. & Wendland, H., 2006, *Acta Numerica*, 15, 543
- Schulz-Rinne, C.W., 1993, *SIAM Journal of Mathematical Analysis*, 24, 76
- Sedov, L.I., 1959, *Proceedings of the Royal Society of London Series A*, New York: Academic Press, 1959
- Shibata, M. & Nakamura, T. 1995, *Phys. Rev. D*, 52, 5428
- Shibata, M., 2016, *Numerical Relativity*, World Scientific

- Springel, V., & Hernquist, L., 2002, *MNRAS*, 333, 649
Springel, V., 2010, *MNRAS*, 401, 791
Taylor, G., 1950, *Proceedings of the Royal Society of London Series A*, 201, 159
Tichy, W. & Marronetti, P., 2007, *Phys. Rev. D*, 76, 061502
Timmes, F. & Swesty, D., 2000, *ApJS*, 126, 501
van Leer, B., 1974, *Journal of Computational Physics*, 14, 361
Vila, J.P., 1999, *Mathematical Models and Methods in Applied Science*, 02, 161
von Neumann, J. & Richtmyer, R.D. 1950, *Journal of Applied Physics*, 21, 232
Wendland, H., 1995, *Advances in Computational Mathematics*, 4, 389